A model for phase balancing and velocity filtering

William S. Harlan

ABSTRACT

Hyperbolic reflections and convolutional wavelets are fundamental models for seismic data processing. Each sample of a "stacked" zero-offset section can parametrize an impulsive hyperbolic reflection in a midpoint gather. Convolutional wavelets can model source waveforms and near-surface filtering at the shot and geophone positions. An optimized inversion of their combined modeling equations makes explicit any inter-dependence and non-uniqueness in these two sets of parameters.

First, I estimate stacked traces that best model the recorded data and then find non-impulsive wavelets to improve the fit with the data. These wavelets are used for a new estimate of the stacked traces, and so on. Estimated stacked traces model short average wavelets with a superposition of approximately parallel hyperbolas; estimated wavelets adjust the phase and amplitudes of inconsistent traces, including static shifts. Deconvolution of land data with estimated wavelets makes wavelets consistent over offset; remaining static shifts are midpoint consistent. This phase balancing improves the resolution of stacked data and of velocity analyses.

If precise velocity functions are not known, then many stacked traces can be inverted simultaneously, each with a different velocity function. However, the increased number of overlain hyperbolas can more easily model the effects of inconsistent wavelets. As a compromise, I limit velocity functions to reasonable regions selected from a semblance velocity analysis--a few functions cover velocities of primary and multiple reflections. Multiple reflections are modeled separately and then subtracted from marine data.

Phase inconsistencies ought also to be recognizable over midpoint. Convolutional wavelets can be constrained with surface-consistency. Alternatively, one can model two-dimensional stacks as a sum of diffraction hyperbolas over midpoint, much as is done over offset. Dip moveout makes the diffraction and normal-moveout velocities equivalent.

INTRODUCTION

Hyperbolic reflections and convolutional wavelets are fundamental models for the processing of seismic data (see Robinson, 1983, for example), yet the two are rarely considered together. Deconvolution can improve the quality of hyperbolic stacks and of semblance velocity analyses by making the recorded seismic wavelets shorter and more consistent from trace to trace. However, deconvolution does not customarily consider its effects on stacking, nor does deconvolution use the information gained by stacking and velocity analysis.

The normal-moveout (NMO) model assumes that the earth's impulse response is a sequence of hyperbolas in common-midpoint (CMP) gathers. Convolution models only wave sources and filtering that are near the surface, linear, time-invariant, and isotropic. Deeper and non-isotropic filtering depends on the path and the angle of incidence of a wave. Convolution cannot model angular changes in reflection coefficients if more than one reflection appears in the data.

For reflections to be expressed as a sum of hyperbolas, root-mean-square (rms) velocities must adequately parametrize the traveltimes of waves. Local seismic velocities must change slowly both vertically and horizontally. Fortunately, a linear superposition of hyperbolic reflections can also model reflections from dipping, curved, and diffracting interfaces.

Static shifts are usually treated independently because they are a simpler special case of the convolutional model. (A static shift is a convolution with a shifted delta function.) Ronen (1985) and Rothman (1986) have shown how to make static corrections directly dependent on the quality of the hyperbolic stack at chosen velocities. Simultaneous (residual) velocity analysis has been difficult, unless structure is assumed flat (Shultz, 1985).

An "NMO correction" of a CMP gather flattens hyperbolic reflections and makes structural information more accessible. Wavelets, on the other hand, are distorted by NMO. Claerbout (1986) suggested simultaneous deconvolution of CMP gathers before and after NMO corrections to distinguish the effects of a source wavelet from that of predictable reflection coefficients (short-period multiples). He concluded that the oversimplicity of NMO corrections as a downward-continuation process limited the ability to discriminate structural and source information.

This paper does not aim immediately to go beyond the assumptions of the hyperbolic and convolutional models, but rather to find the simplest means of considering the two together. Instead of defining the stacked section and deconvolution wavelets

directly, I shall treat them as parameters in equations that model the data. Inversion of the equations by optimization then requires considering the effect of each process on the other.

The common procedure of "velocity filtering" attempts to suppress multiples from CMP gathers by linear filtering along carefully chosen hyperbolic paths. Hutchinson and Link (1984) and Thorson and Claerbout (1985) demonstrated that multiple reflections are better suppressed by first modeling them with a superposition of hyperbolas and then subtracting them from the data. The addition of independent wavelets for each trace should increase the accuracy of modeled reflections.

A damped least-squares objective function will be minimized by iterative estimates of the parameters with a conjugate-gradient algorithm. Accurate estimation of stacking velocities will be made unnecessary by including a number of stacks with different stacking velocity functions.

ASSUMPTIONS OF THE NORMAL MOVEOUT AND CONVOLUTIONAL MODELS

A hyperbolic normal-moveout (NMO) equation makes very restrictive physical assumptions, but it can be extended for more complicated reflections. Common midpoint (CMP) gathers include all shot positions, s, and geophone positions, g, with identical midpoint coordinates, $y = (s+g)/2$. Each gather is arranged by the offset coordinate $h = (g-s)$. If an impulsive source passes through a medium of constant velocity v and reflects off a flat reflector, then the traveltime t is given by the following moveout equation:

$$t^2 = t_0^2 + \frac{h^2}{v^2} \quad . \tag{1}$$

t_0 is the traveltime at zero offset.

For a dipping layer, the equation remains exact if v is set equal to the constant velocity divided by the cosine of the layer's dip (Levin, 1971). Alternatively, reflection times from a horizontally stratified medium (layers are flat; velocity changes only vertically) can be approximated to second order in h if v is replaced by the root-mean-square (rms) velocity:

$$[v_{rms}(z)]^2 = \frac{\int_0^z v(z')dz'}{\int_0^z [v(z')]^{-1}dz'} \quad , \tag{2}$$

where z is the vertical depth. A combination of the dip correction and rms velocity is

common.

A convolutional model is, by definition, linear and time-invariant. Convolutions cannot depend on the raypath or on the angle of arrival because these parameters change with time. All such filtering must occur isotropically at the surface, the only points common to all raypaths. The NMO model assumes that the data represent an impulse response; that is, the shots and geophones have impulsive radiation patterns. Surface-consistent convolution assumes that the earth's impulse response has been filtered independently at the shot and geophone positions to create the recorded data:

$$\text{data}(s\,,g\,,t\,) = \text{impulse}(s\,,g\,,t\,) \;*\; w_s(s\,,t\,) \;*\; w_g(g\,,t\,)\;.$$

The stars indicate convolution over time. $w_s(s\,,t\,)$ models the shot waveform as filtered by the near surface; $w_g(g\,,t\,)$ models filtering at and by the geophone. If one considers only a single midpoint gather at at y_0, then

$$\text{data}(h\,,t\,) = \text{impulse}(h\,,t\,) \;*\; w(h\,,t\,)\;,$$

$$\text{where } w(h\,,t\,) = w_s(s\;=y_0-h\,,t\,) \;*\; w_g(g\;=y_0+h\;,\;t\,)\quad. \tag{3}$$

The wavelets $w(h\,,t\,)$ share no common surface-consistent wavelets.

The usual goals of these two models is (prestack) deconvolution and the NMO stack. To see the implicit constraints on the data, one can imagine reversing the normal processing sequence to reconstruct the data from the stacked data and convolutional wavelets.

Imagine that a stacked seismic profile represents (as post-stack migration assumes) a zero-offset impulse response. Each stacked trace can be stretched according to its NMO velocity function to model an entire midpoint gather. The stack does not preserve information on changes in amplitude and phase with offset, so the stretching must make simple assumptions on the geometric spreading of reflections, frequency absorption, and changes in reflection coefficient with angle. If more than one stacked section is available, then one can sum their modeled gathers to create reflections, such as primaries and multiples, that arrive simultaneously with inconsistent velocities. Finally, each trace can be convolved with corresponding wavelets. This sequence of steps will be defined next with simple modeling equations.

A MODEL FOR MIDPOINT GATHERS

Let us begin with a model for a single midpoint gather. Choose a set of rms velocity functions $v_j(t_0)$ that cover all reasonable primary and multiple velocities. Let $r_j(t_0)$ be the corresponding "deconvolved, stacked" traces that parametrize the amplitudes and zero-offset arrival times of reflections--call them reflectivity functions. The following equation maps each point of a reflectivity function to a hyperbola over offset:

$$\text{hyp}_1(h,t) = \sum_j \int \delta[t - \sqrt{t_0^2 - h^2/v_j^2(t_0)}]\, r_j(t_0)\, dt_0 \quad . \tag{4}$$

If the reflectivity function contains an impulsive delta function, then the impulsive hyperbolic reflection is constant in strength over offset. This model is similar to that used by Thorson and Claerbout (1985). They express the zero-offset traveltime in the reflectivity as a function of the traveltime (with some differences in amplitudes) and use a continuous range of constant velocities.

For sampled data, function (4) will be convolved by a stretched sin(t)/t function (a sinc function) that is bandlimited to the Nyquist frequency of the data (see Bracewell, 1978). Equivalently one can replace the delta function in equation (4) by a sinc.

As an simple example, the reflectivity functions in figure 1a are mapped to the hyperbolas of figure 2a. The two non-zero reflectivity functions correspond to constant velocities of 1.4 and 2 (labeled in squared reciprocal velocity, or squared slowness). Only three nonzero samples (reflections) appear--two with the same velocity, two with the same zero-offset traveltime. Note that the length and amplitude of the sinc wavelet is constant with offset, unlike an NMO stretched wavelet.

To model one common-midpoint gather, convolve each trace of the hyperbolic reflections in (4) with a wavelet:

$$\hat{\text{data}}_1(h,t) = w(h,t) * \text{hyp}_1(h,t)\ ;$$

$$\text{or}\quad \hat{\text{data}}_1(h, t=t') = \sum_j \int w\,[h,\ t=t' - \sqrt{t_0^2 + h^2/v_j^2(t_0)}\ ]\ r_j(t_0)\, dt_0 \quad . \tag{5}$$

Clearly, this modeling equation is not completely invertible. The transformation destroys information in the phase and amplitude spectrums of the convolutional wavelets and reflectivity functions. For instance, the phase of the reflectivity functions and wavelets could be simultaneously reversed without affecting the modeled data. Frequencies missing from wavelets will be difficult to recover in the reflectivity without using statistical constraints.

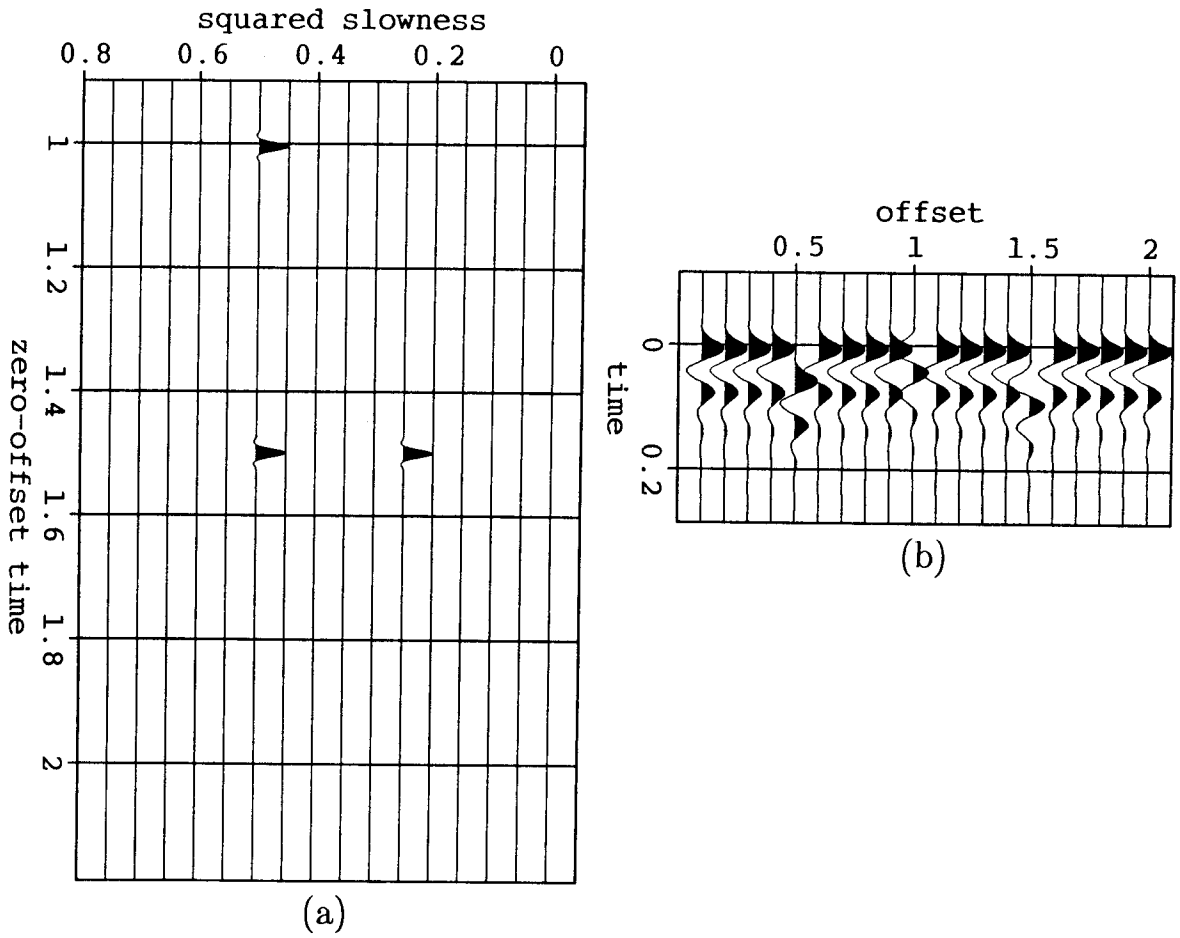

FIG. 1. (a) Two non-zero reflectivity functions with velocities of 1.4 and 2 (squared slownesses of 0.5 and 0.25). (b) Convolutional wavelets, three of which are inconsistent in phase.

Figure 1b contains a set of convolutional wavelets; three are inconsistent in phase. Figure 2b shows the convolution of these wavelets with the corresponding traces of figure 2a. Many high frequencies are lost, and the zero-offset traveltimes of the reflections are more ambiguous.

Some problems posed by one-dimensional deconvolution can be ameliorated by inversion of the two-dimensional model. Any single trace of figure 2b could be regarded as having a lengthy wavelet and one reflection coefficient. One could also subdivide a wavelet and claim more than three reflections. Because different hyperbolic reflections converge with increasing offset, inversion of the two-dimensional model can avoid fewer than three reflections by encouraging wavelets to be as consistent as possible. Within a

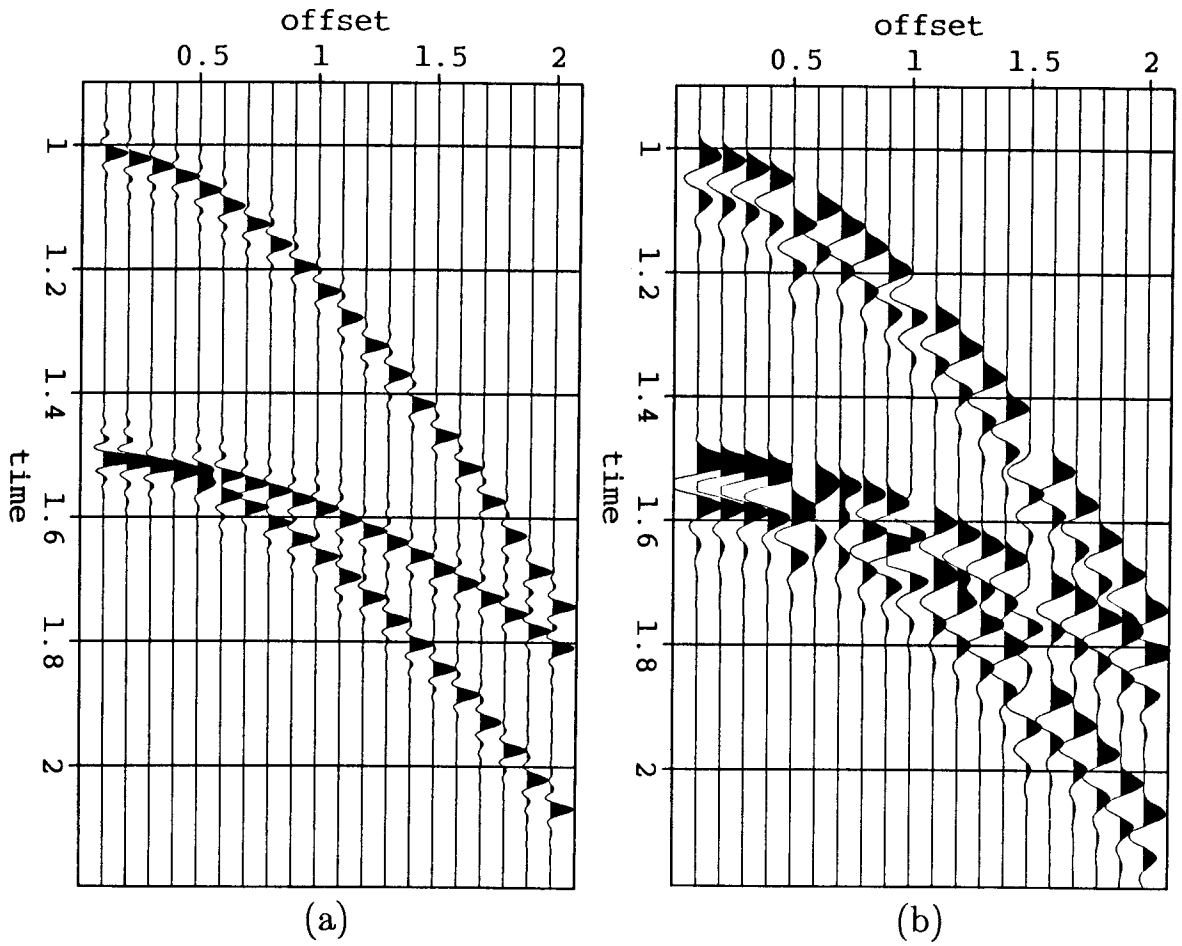

FIG. 2. (a) Three hyperbolic reflections modeled from equation (4) and the reflectivity functions in figure 1a. Convolution with sinc functions avoids aliasing. (b) A convolution of the reflections in (a) with the wavelets in figure 1b. High frequency information is lost, and zero-offset arrival times are more ambiguous.

single reflection, the lobes of long consistent wavelets remain parallel--an easier appearance to model with convolution than with reflections at different velocities. Statistical methods of one-dimensional deconvolution might tell us that three reflections were most probable, depending on the assumptions. But with more complicated wavelets and reflection sequences, the difficulties of one-dimensional deconvolution would increase.

The NMO equation (1) describes only the initial arrival times of the wavelets, not the tails. The best-fitting hyperbola to the tails of wavelets corresponds to a lower velocity than a hyperbola fitting the first arrival times. This difference in velocity is small when wavelets are short, so a reflectivity function can still model much of the phase of consistent short wavelets.

AN OBJECTIVE FUNCTION

Optimization methods improve endlessly, so let us first define an inversion of (5) in terms of an objective function rather than by a specific algorithm. This function measures the least-squares error between the recorded and modeled data and constrains the unknowns with two penalty functions (scaled by small constants a_r and a_w) to insure stability:

$$J = \int\int [\text{error}(h,t)]^2 dh dt + a_r \sum_j \int [r_j(t_0)]^2 dt_0 + a_w \int\int [w(h,t)]^2 \, dh dt \ ,$$

$$\text{where} \quad \text{error}(h,t) = \text{data}(h,t) - \hat{\text{data}}_1(h,t) \ . \tag{6}$$

The optimal $r_j(t_0)$ and $w(h,t)$ should minimize J. (For convenience I shall continue to write s, g, y, and h as continuous variables. Their integrals can in all cases be replaced by a sum over sampled data points.) The effect of the two penalty functions can be compared to adding a small constant to the diagonal of a possibly singular matrix before inversion (prewhitening).

Note that J is a quadratic function of the reflectivity function or of the wavelets, but not of an array that contains both functions. Thus, quadratic optimization methods, such as conjugate-gradient descent (Luenberger, 1984) can minimize the two functions independently, but not simultaneously. If the wavelets are not allowed to change, then the optimum reflectivities are a linear function of the error, and vice versa.

Minimizing this least-squares objective function equivalently maximizes the probability of the data, assuming that noise, the reflectivity, and the wavelets are all Gaussian and white (see Kendall and Stuart, 1979, for example). More justifiable statistical assumptions can be imagined, but the quadratic form is a convenient first choice.

OPTIMIZATION

Quadratic objective functions are ideal for gradient-descent methods of optimization because the required gradients are linear functions of the data. The gradient of the objective function with respect to the wavelet function (array) includes a correlation of the data error defined by equation (6) and the impulsive hyperbolas modeled by equation (4):

$$\frac{\delta J}{\delta w(h, t=t')} = -\int\int \text{hyp}_1(h, t = t''-t') \, \text{error}(h, t = t'') dt'' + a_w \, w(h, t=t') \ . \tag{7}$$

The penalty term on the energy of the wavelet adds a term proportional to the reference

value of the wavelet.

The gradient with respect to the reflectivity includes an NMO stack that uses the reference wavelets as interpolation functions:

$$\frac{\delta J}{\delta r_j(t_0)} =$$

$$-\int\int w\,[h, t = t' - \sqrt{t_0^2 + h^2/v_j(t_0)^2}\,]\ \text{error}(h, t = t')\,dt'\,dh + a_r\ r_j(t_0) \quad . \qquad (8)$$

If objective function (6) has a broad flat minimum, then gradient descent methods cannot reach the vicinity of the global minimum in a small number of steps. The parameter penalty functions will not much affect the results of an incomplete optimization. Different optimization methods will, in practice, constrain the solution differently.

A simultaneous steepest-descent perturbation of both sets of parameters unfortunately requires an expensive line search to scale the combined gradients (7) and (8). If, however, either parameter is optimized independently, the necessary scale factor can be calculated from simple dot products (see Luenberger, 1984, on quadratic objective functions).

I optimize objective function (6) alternately with respect to the wavelets and reflectivity:

1. Assume that wavelets are impulse functions with zero lag and find the optimum reflectivity functions.
2. Leaving reflectivity functions unchanged, find the optimum wavelets. If unsatisfied, go on.
3. Re-estimate the reflectivity functions with the new wavelets, then return to step 2.

Each step solves an overdetermined least-squares problem. This procedure has little chance of optimizing the objective function completely. The first estimated wavelets will explain only what the reflectivity cannot; the next estimate of the reflectivity explains what these wavelets cannot, and so on. The procedure will not work at all if phases are too inconsistent: step 1 will be unable to fit anything with hyperbolas and step 2 will have nothing to improve upon.

The reflectivity and wavelets in figures 3a and 3b were estimated by three such cycles. Each least-squares optimization used four conjugate-gradient steps. The modeled data are barely distinguishable from the original data when plotted on the same scale. The energy (the sum of squared amplitudes) of the difference between the modeled and original data is 1% the energy of the original data.

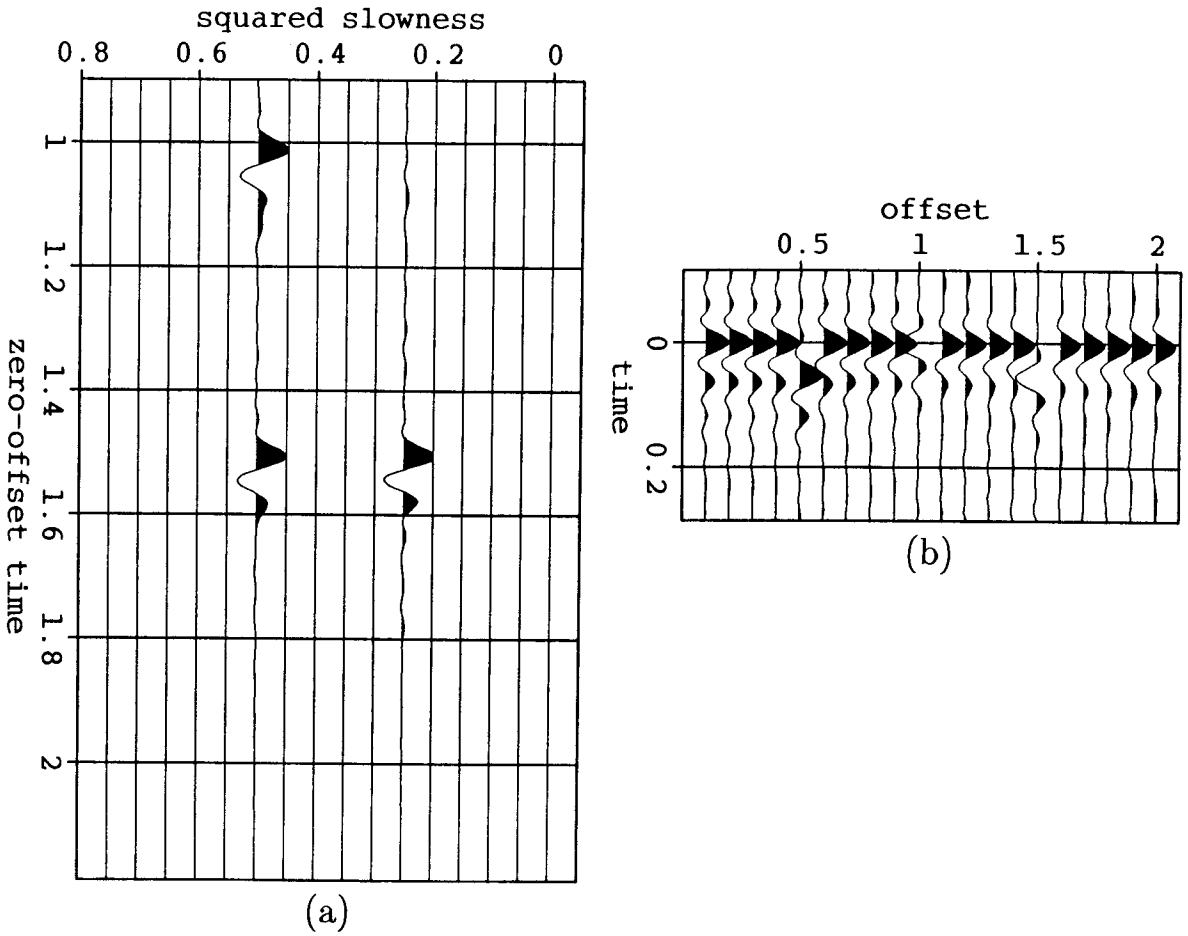

FIG. 3. (a) Estimated reflectivity functions from minimization of objective function (6). (b) Corresponding estimated convolutional wavelets. Reflectivity functions model the average phase of the reflections; estimated wavelets have approximately zero phase and differ only to adjust inconsistent traces. The modeled and original data are barely distinguishable.

The three reflections appear in the reflectivity functions with the average phase and amplitude of the wavelets, unlike the original impulses. The estimated wavelets are approximately zero-phase after time shifting, unlike the original wavelets. The reflectivity functions model a consistent average wavelet with a superposition of approximately parallel hyperbolas. As expected, the estimated wavelets model only relative changes in phase and amplitude that cannot be modeled by the reflectivity. Because hyperbolas at a single velocity converge at high offsets, reflectivity could not model wavelets of indefinite length.

PHASE-BALANCING DECONVOLUTION

Assuming that the estimated wavelets express *relative* changes in phase and amplitude, one can use them to estimate what data would have resulted from a single consistent wavelet (although unknown). Such a process can be called phase balancing. To partially invert the convolution with known wavelets, minimize the following damped least-squares objective function:

$$\min_{\text{decon}(h\,,t\,)} \int\int [\text{data}(h\,,t\,) - \text{decon}(h\,,t\,) * w(h\,,t\,)]^2 dh dt + a_d \int\int [\text{decon}(h\,,t\,)]^2 dh dt. \quad (9)$$

The gradient of this objective function with respect to the deconvolved data, decon$(h\,,t\,)$, includes a correlation of the known wavelet with the difference between the original and modeled data. Again, four conjugate-gradient steps were used. Figure 4 shows the result of deconvolving the original data of figure 2b with the estimated wavelets of figure 3b.

This deconvolved gather is far from the ideal impulsive reflections of figure 2a, but the wavelets are now consistent. A second "spiking" deconvolution could use the same wavelet for all traces. Consistent wavelets are also essential if one is interested in angular (not convolutional) changes in reflection coefficients.

INVERSION WITH UNCONSTRAINED AND APPROXIMATE VELOCITIES

The preceding example demonstrates that information about the absolute phase of wavelets is lost in the data modeled by equation (5). In fact, some information is also lost about relative differences between wavelets when stacking velocities cannot be chosen with precision.

Processing of midpoint gathers customarily begins with a semblance velocity analysis. The following equation evaluated the semblance panel in figure 5a from the data in figure 2b:

$$\text{semb}(m\,,t_0) = \frac{[\int \text{data}(h\,,t = \sqrt{{t_0}^2 + m h^2}) dh\,]^2}{\int [\text{data}(h\,,t = \sqrt{{t_0}^2 + m h^2})]^2 dh} \quad . \quad (10)$$

The squared slowness, $m = 1/v^2$, has the useful property that the resolution is approximately the same at both high and low values. The panel ranges over squared slownesses of 0.75 to 0, and velocities of 1.2 to infinity. The sixth and eleventh traces correspond to the two velocities used in the original model.

The panel shows high semblances at incorrect velocities. Even zero slowness (infinite velocity) has a substantial amplitude. One cannot expect to choose perfect

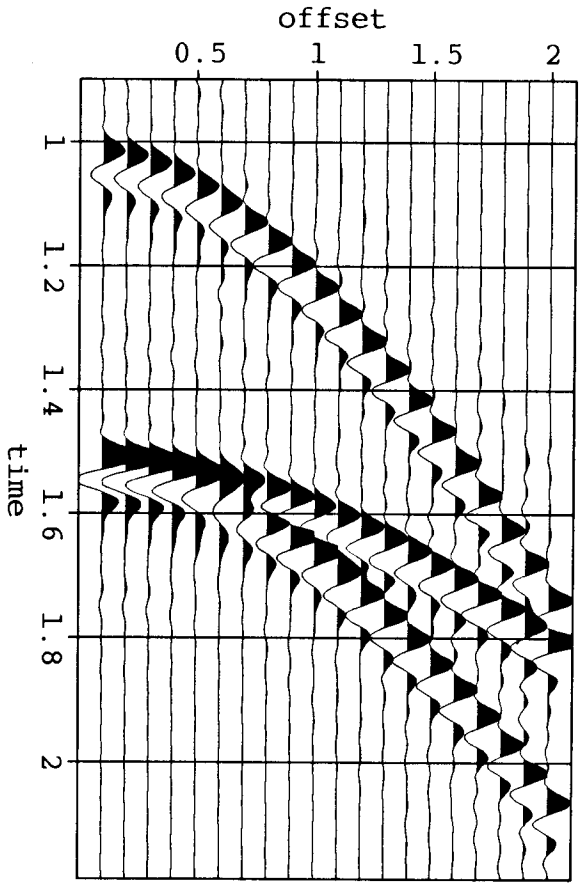

FIG. 4. A deconvolution of the data in figure 2b with the estimated wavelets in figure 3b. Reflections are not impulsive as in the ideal data of figure 2a, but wavelets are now consistent.

velocity functions for reflections from this panel, though one can place reasonable limits on their values.

Even more dramatic is the result of stacking the data over the same range of velocities. Each trace of figure 5b was created by summing the data over offset along hyperbolas with the corresponding zero-offset time and slowness. Because all hyperbolas have low dip at low offsets, all stacks show substantial amplitudes at incorrect velocities. This can be bad or good depending on whether one wants a stack to discriminate against bad velocities or to see as many reflections as possible.

To test an extreme case, I invert model (5) with velocity functions that lie over the same range of squared slownesses as the semblance panel:

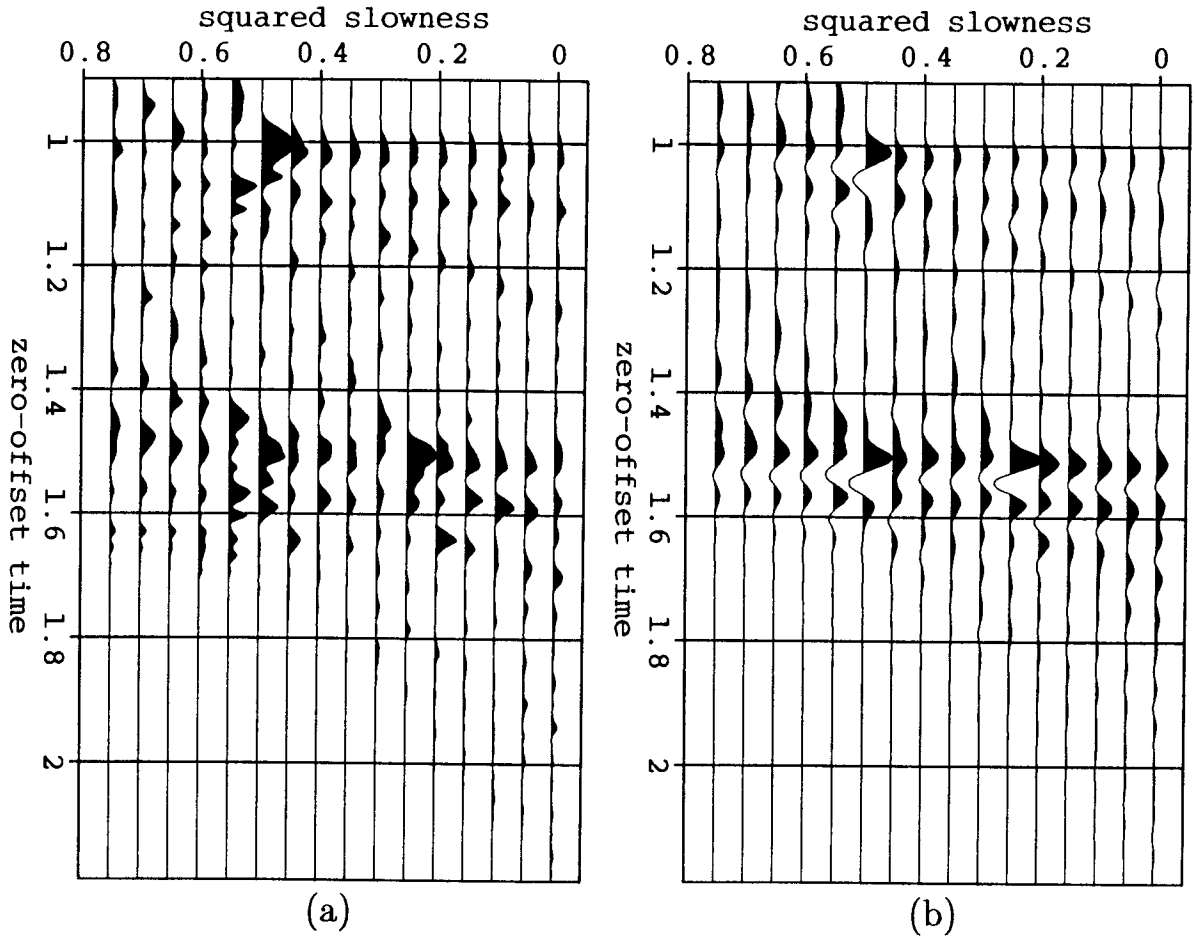

FIG. 5. (a) A hyperbolic semblance stack of the data in figure 2b. Traces are sampled evenly over squared slowness (the reciprocal of squared velocity). (b) An additive stack of the data over the same range of velocities. Amplitudes are high at incorrect velocities because of the similarity of hyperbolas at low offsets.

$$1/[v_i(t_0)]^2 = m_0 + i\,\Delta m \;\; ; \quad m_0 = 0.75; \quad \text{and } \Delta m = -0.05 \; .$$

The corresponding estimated reflectivity functions appear in figure 6a. Note that much energy appears in traces with incorrect velocities, though not as much as in the stack in figure 5b. Reflectivity functions discriminate against reflections with incorrect velocities better than does a stack because the former must describe reflections at all offsets. This panel of reflectivity functions could be used as a velocity analysis that preserves phase information: a slice through the panel at the best velocities gives the optimum stack.

When combined with the convolutional wavelets in figure 6b, these reflectivity functions model the data as well as do the more constrained results in figure 3. The

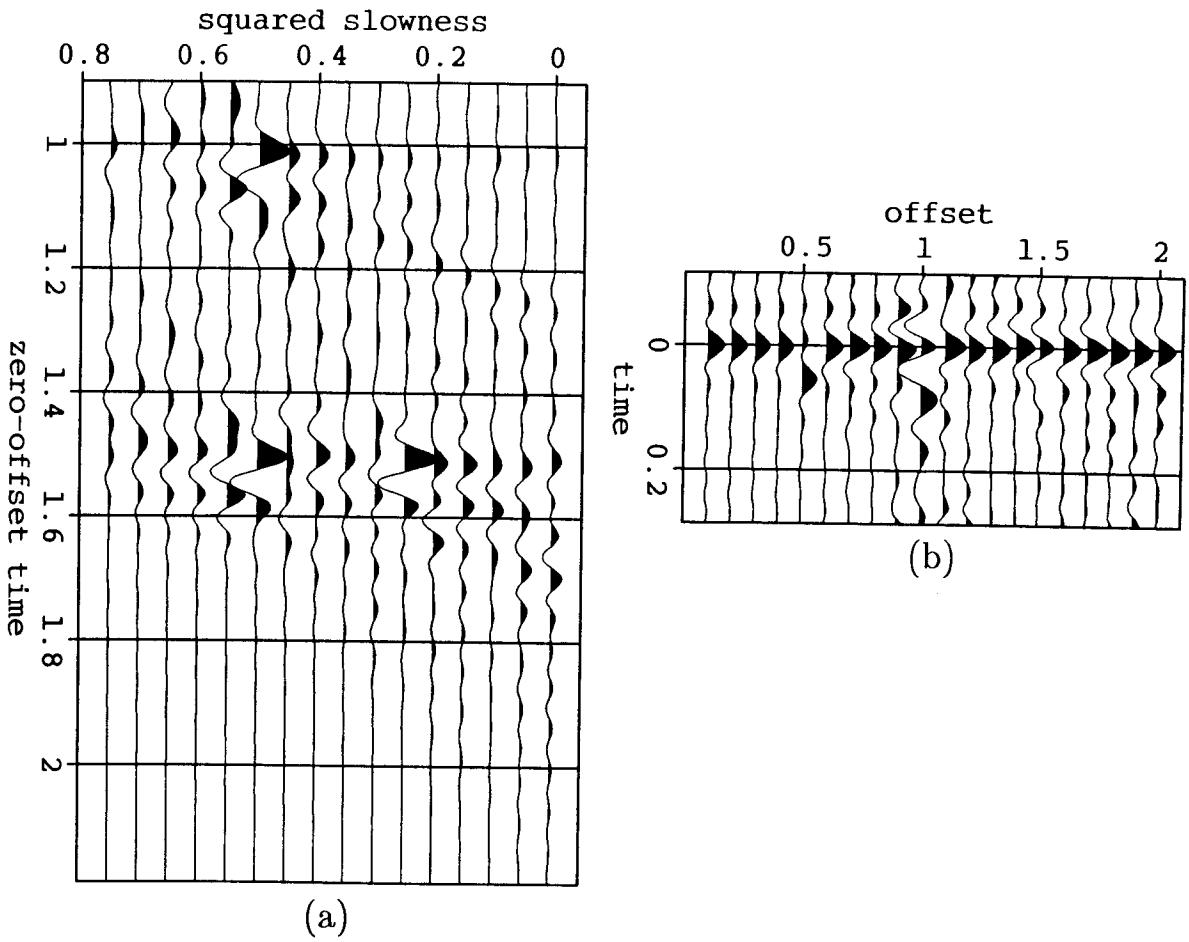

FIG. 6. (a) Estimated reflectivity functions over the same range of velocities as the stacks in figure 5. (b) Corresponding convolutional wavelets. These estimates model data as well as the results in figure 3. Wavelets no longer accurately model inconsistent phase at high offsets because the additional overlapping hyperbolas can also model these differences.

greater number of variables has increased the nonuniqueness of the modeling equation (5). The inconsistent wavelets have been estimated poorly, particularly at high offsets, because the greater number of overlapping hyperbolas can also model these differences.

The two extremes of these synthetic examples suggest the following rule: the more constraints placed on the velocities of reflections, the easier it is to recognize inconsistent wavelets at high offsets. (Note that surface-consistent shot and geophone wavelets affect both high and low offsets in different midpoint gathers.)

As a compromise, three velocity functions were chosen about each of the two correct velocities. The estimated reflectivity functions in figure 7a show large amplitudes

at the incorrect velocities. Again the modeled data are very good. This time, however, the estimated wavelets in figure 7b are only slightly inferior to those of the well-constrained estimate in figure 3b. A perfect knowledge of velocities would then seem to be unnecessary to estimate relative changes in convolutional filtering from trace to trace.

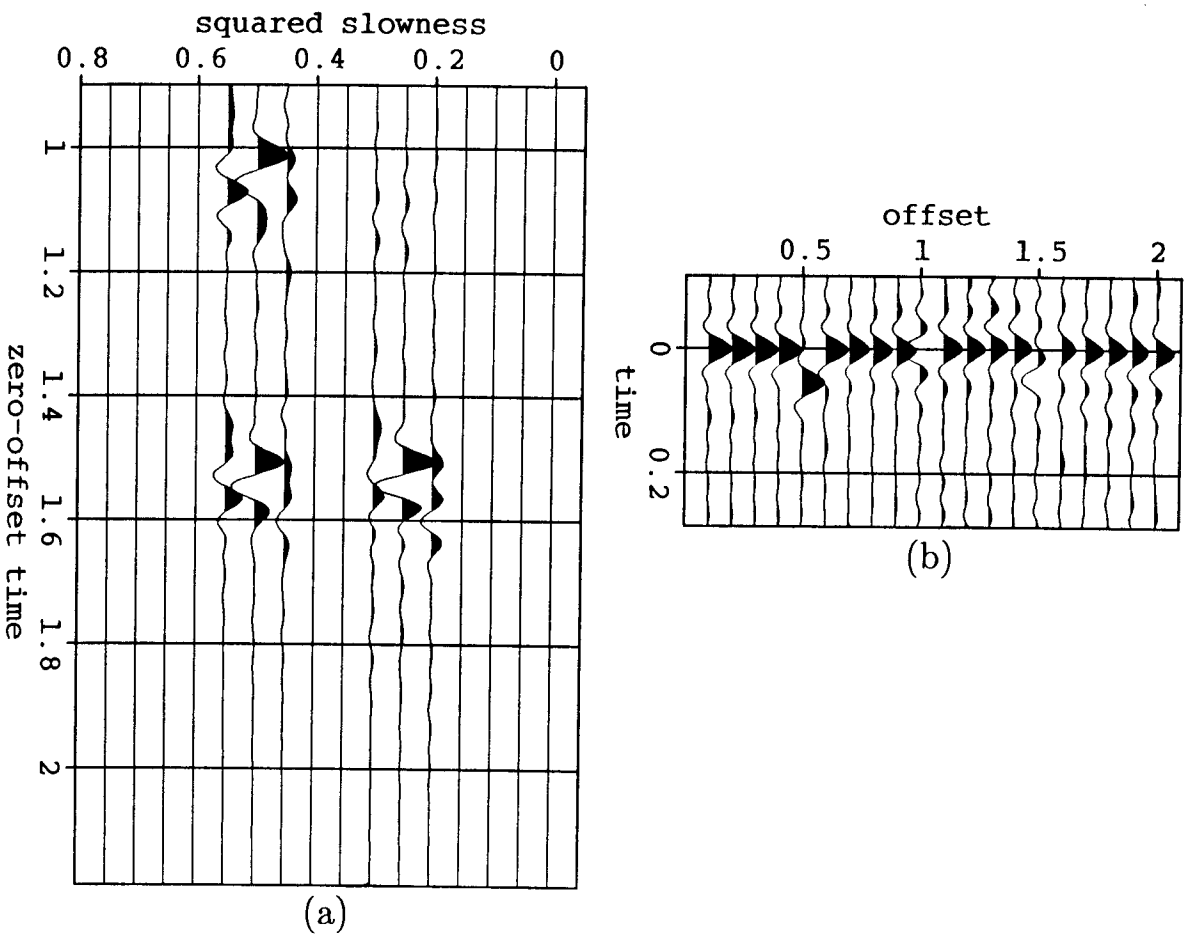

FIG. 7. (a) Estimated reflectivity functions at six velocities near the correct values. (b) Corresponding estimated convolutional wavelets. Substantial amplitudes appear at incorrect velocities in reflectivity functions, but wavelets now model changes in phase as well as did the more constrained estimates in figure 3.

VELOCITY FILTERING

To demonstrate loose constraints on velocities, I use the recorded marine midpoint gather in Figure 8a (provided by the Geophysical Research Institute in Zhuoxian China). Most of the reflections are sea-bottom primaries and multiples with velocities near that of water. The last strong reflection is a pegleg multiple of the primary reflection arriving at zero offset in 1.8s. The strength and phase of wavelets show some change with offset. Amplitudes of traces have been scaled with time to compensate for the effects of geometric spreading and the absorption of energy.

Ten velocity functions were chosen through the semblance contour plot in Figure 8b. The first five functions pass through the water velocity reflections (the first is a primary); the second five pass through higher velocity reflections. The corresponding reflectivity functions and wavelets were estimated with the same algorithm used for the synthetic examples. The modeled data appear in figure 9a. The difference between figures 8a and 9a shows the uninverted reflections in figure 9b. Higher frequencies were uninverted in the first arrivals, perhaps because the wavelets were not allowed to change their spectra with time. Other previously unseen reflections with high velocities appear in the residuals between 2s and 2.5s. These reflections appear as small peaks in the semblance panel of figure 8b, but they were not included in the velocity functions.

Because the lower and higher velocity reflections are not of equal interest, I model the data again in figure 10a with only the five lower-velocity reflectivity functions. Figure 10b shows the original data minus these low-velocity reflections. The remaining data contain the high velocity reflections as well as all uninverted reflections. One can now view the weaker primary reflections without the distraction of water-bottom reflections.

REMOVING STATIC SHIFTS BY PHASE BALANCING

The preceding marine-data example emphasizes the use of reflectivity information to distinguish reflections with different velocities. Convolutions were necessary only to model reflections with greater accuracy than do impulsive hyperbolas alone. Land data are less likely to have multiple reflections than do marine data; instead, filtering at the earth's weathered surface is more likely to create static time shifts such as seen in the midpoint gather in figure 11. (These data were recorded in the Williston Basin by Western Geophysical.) The roughly hyperbolic shapes of the reflections are distorted by static time shifts of traces up and down. The shifted traces contribute destructively to hyperbolic stacks of the data over offset. The mind's ability to imagine hyperbolic reflections makes the static shifts visible to the eye. Similarly, constraints on the hyperbolic shapes of reflections help estimate the wavelets that describe these shifts.

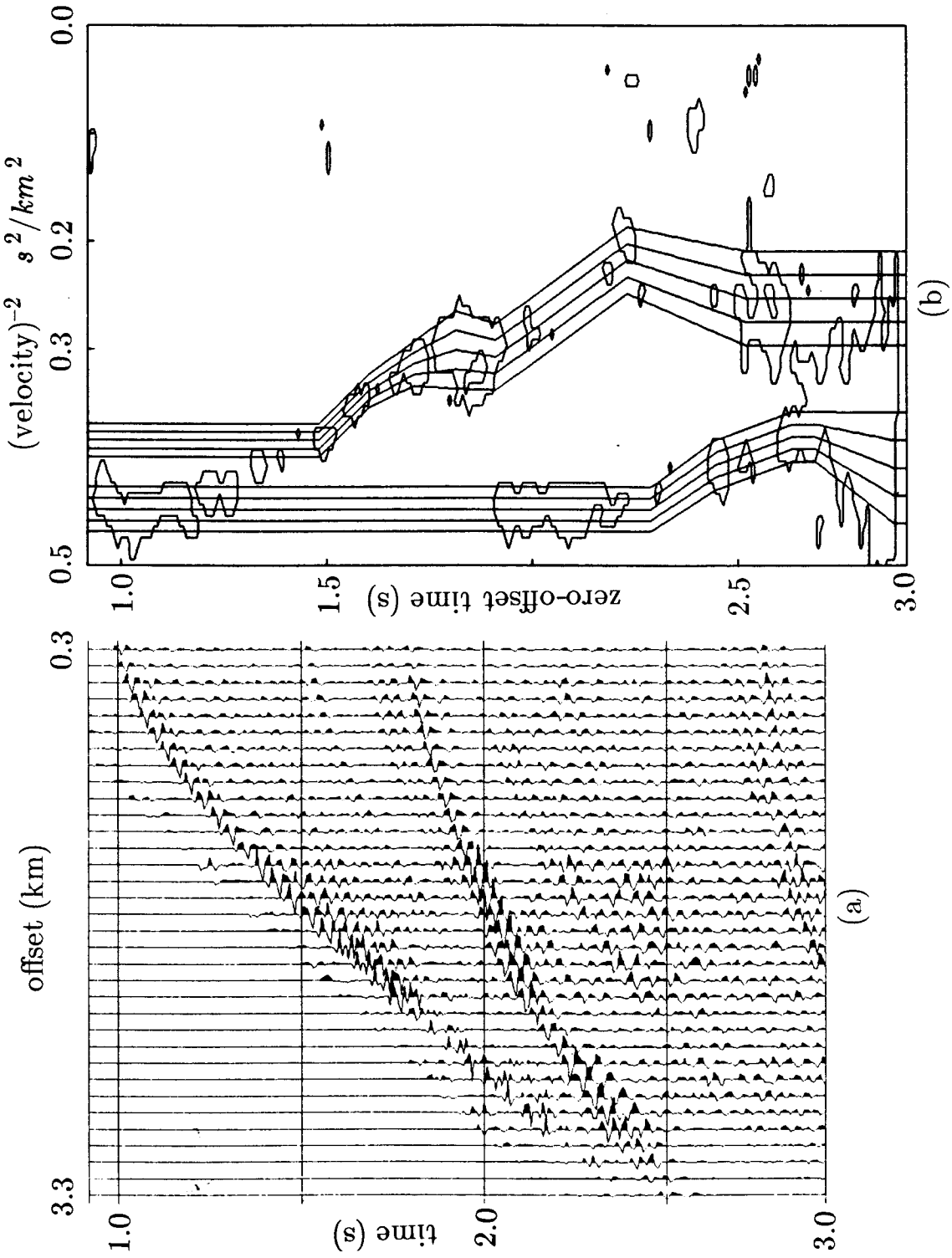

FIG. 8. (a) A marine midpoint gather provided by the Geophysical Research Institute in Zhuoxian China. The last strong reflection is a pegleg multiple of the primary reflection arriving at zero offset in 1.8s. (b) A contour plot of a semblance velocity analysis of (a). Five chosen velocity functions pass through water-velocity reflections; another five pass through higher velocity primaries.

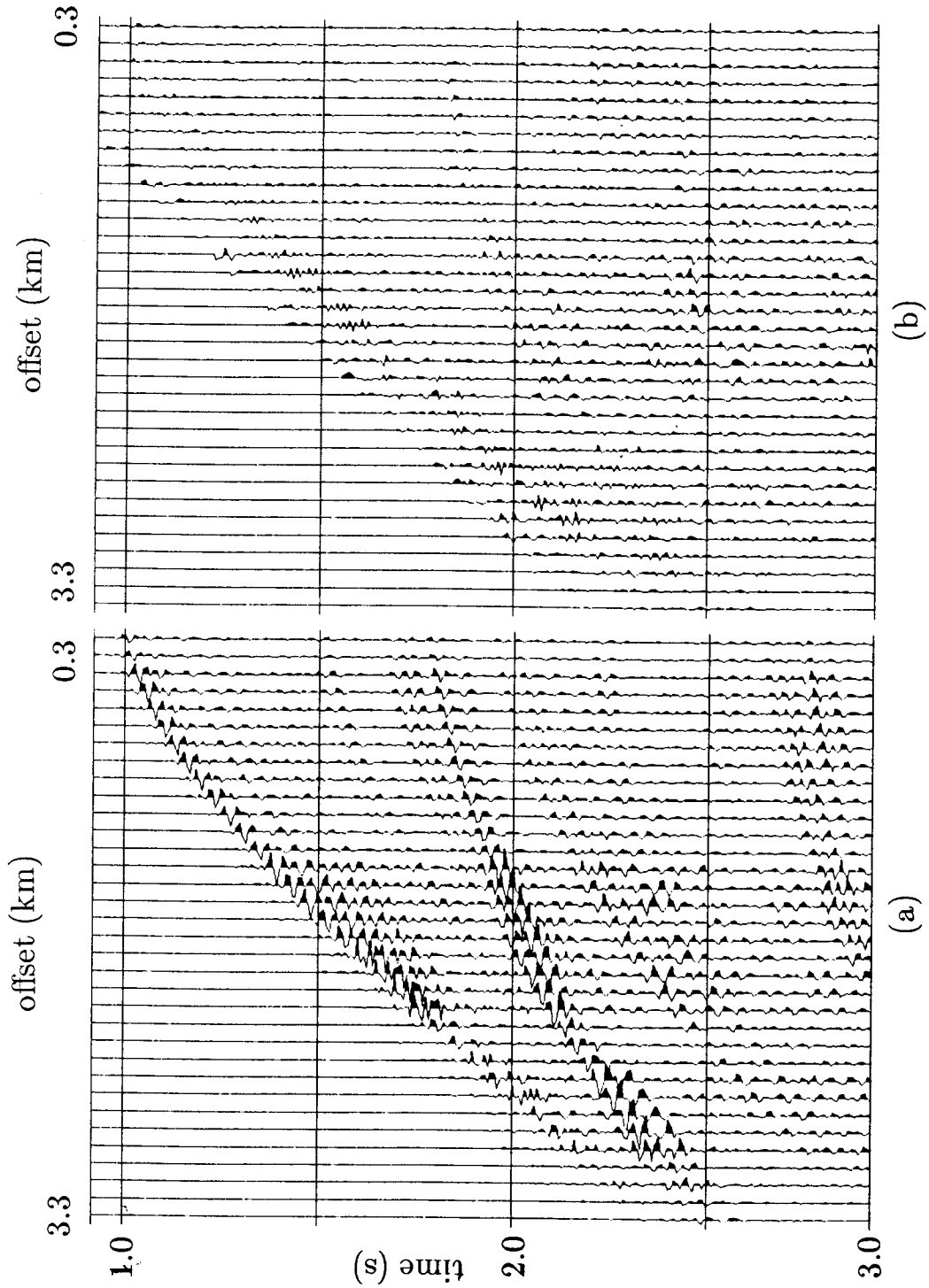

FIG. 9. (a) Reflections modeled by estimated reflectivity and convolutional wavelets. (b) The difference between the recorded data in figure 8a and the modeled data in (a). Reflections with high velocities not included in the model appear between 2s and 2.5s.

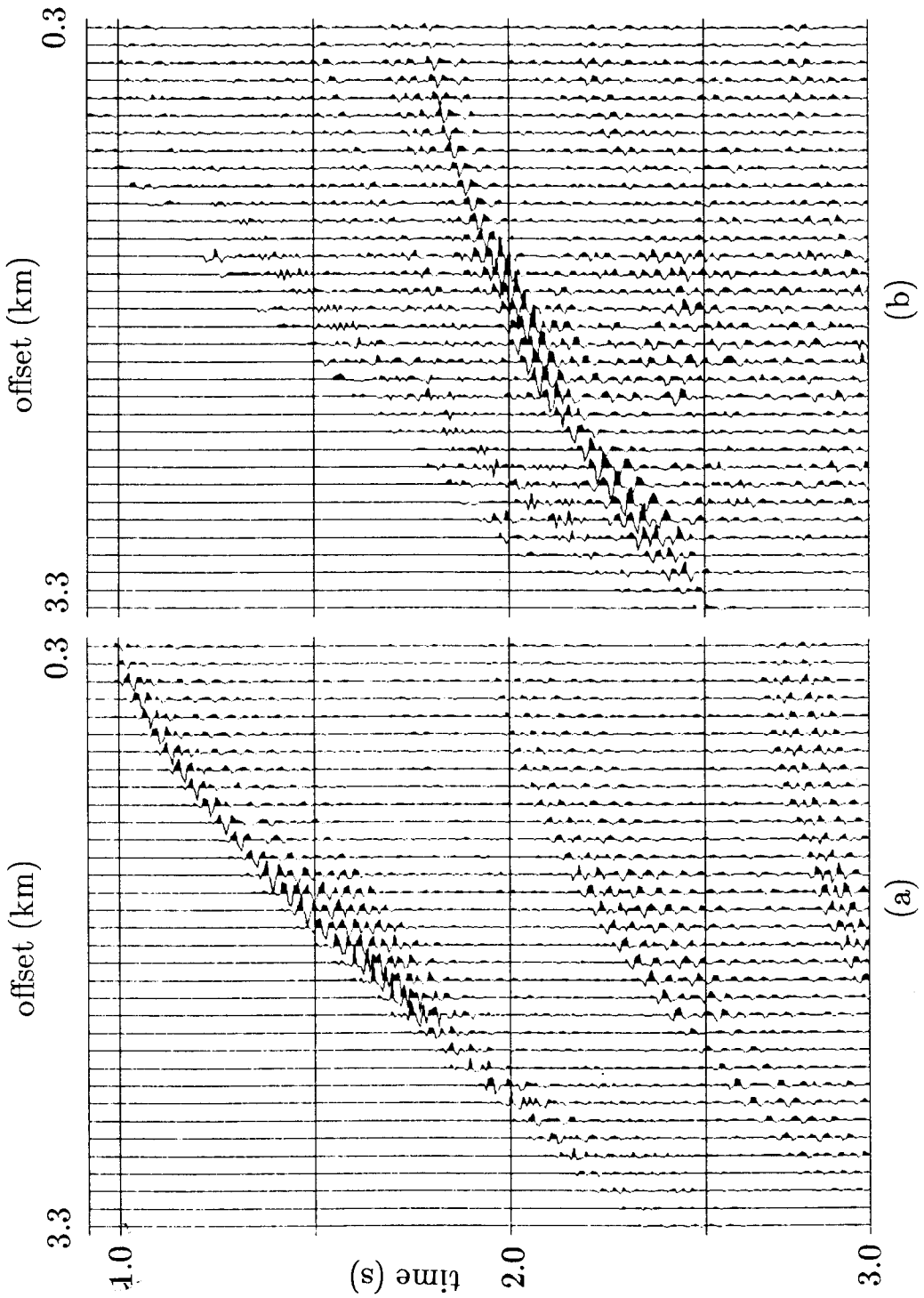

FIG. 10. (a) Reflections modeled only by the five lower velocity functions. (b) The difference between the recorded data (figure 8a) and (a). Weaker primary reflections become more visible.

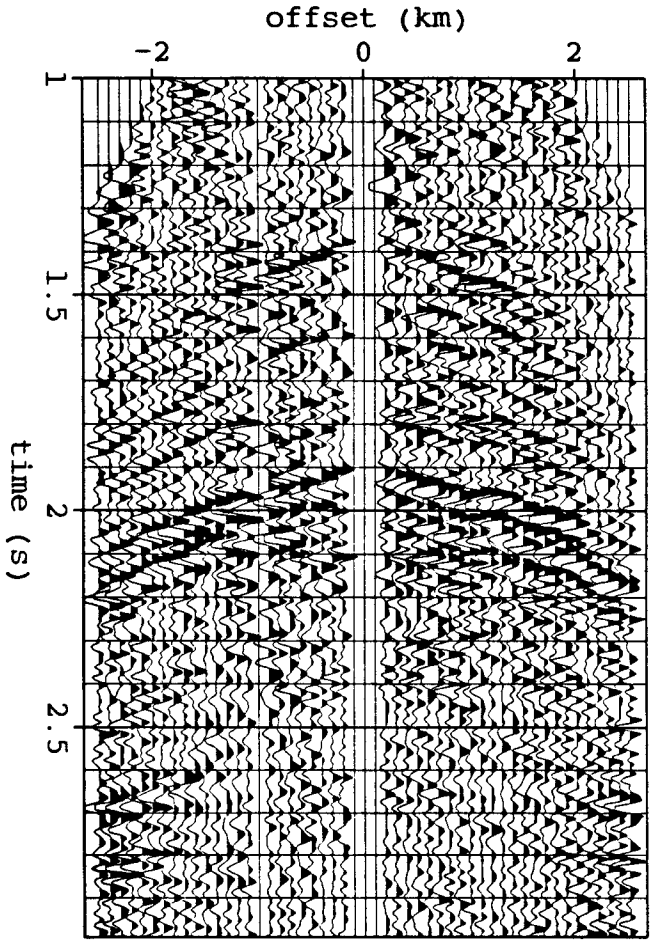

FIG. 11. A midpoint gather recorded on land in the Williston basin (provided by Western Geophysical). Reflections are severely distorted at the uneven surface by static time shifts.

Automatic picking of velocity functions

Since the exact modeling of reflections is less important now than estimating the inconsistent filtering of traces, a single optimum velocity function is used. This function is chosen for each midpoint gather--a troublesome job if done by hand. Instead, a modified version of Toldi's (1985) one-dimensional "velocity analysis without picking" is used.

First, a semblance velocity stack is calculated for each gather, as in figure 12. (The numerator and denominator of the semblance equation (10) are smoothed by convolution with a windowing function approximately the length of the wavelet.) A relatively optimum stacking velocity function (also shown in figure 12) would pass through as

many of these peaks as possible, maximizing the line integral of the semblance along the path. The velocity function still requires some constraints of smoothness and continuity.

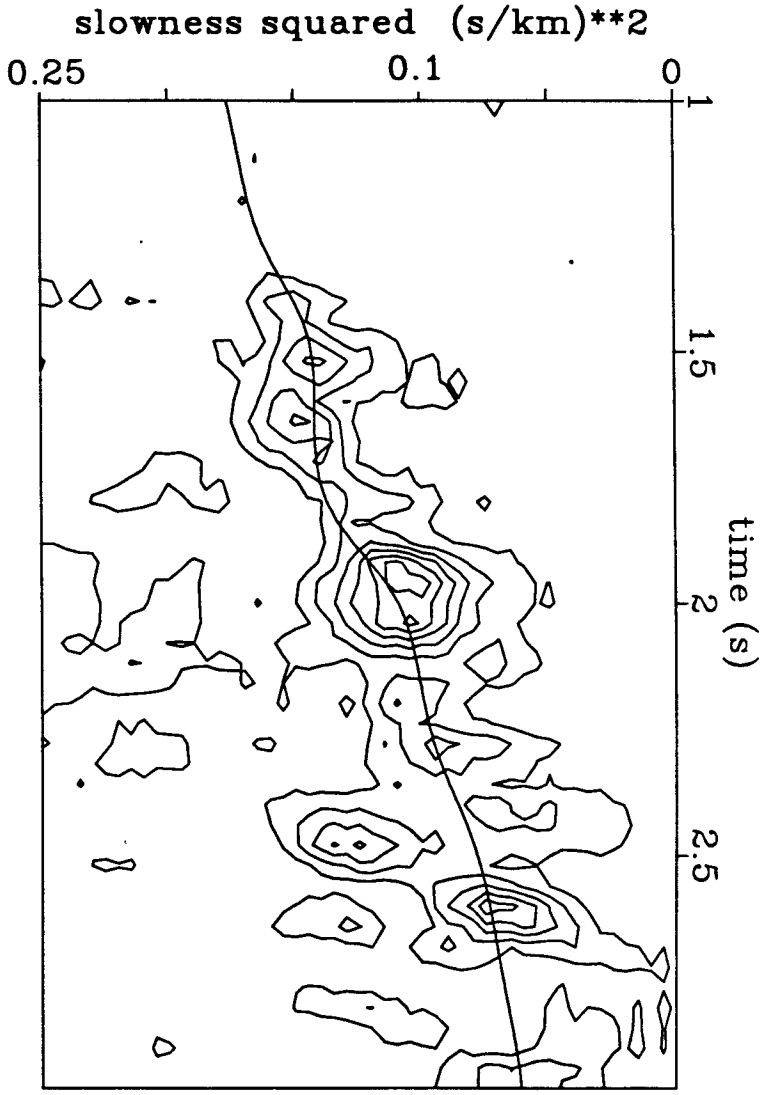

FIG. 12. A hyperbolic semblance stack of the data in figure 11 appears as a function of squared slowness (squared reciprocal velocity) and zero-offset time. An automatically picked velocity function passes through the largest peaks in the panel.

Toldi used the one-dimensional rms velocity equation (2) to parametrize the stacking velocity. A small but abrupt change in rms velocities can correspond to an enormous change in interval velocities. Limiting the range of acceptable interval velocities will encourage smoothness in the rms velocity function. Physical constraints on interval velocities also encourage rms/stacking velocities to describe only useful primary reflections and not multiple reflections and noise. Let us then find an interval velocity function whose corresponding rms squared slowness maximizes the total semblance:

$$\max_{v(t_0)} \int \text{semb}(m = \{\frac{1}{t_0}\int_0^{t_0} [v(t_0')]^2 dt_0'\}^{-1},\ t_0) dt_0 \ . \tag{11}$$

Semblance stacks do not contain information about abrupt changes in interval velocities with depth, so there is no point in allowing them in our model. Toldi measured the smoothness of the estimated interval velocities with a penalty term that integrated the square of the velocity function's derivatives. This penalty term was added to the objective function (11) with a scaling factor that decided the relative weight given to smoothness and total semblance. If an assumed amount of smoothness (a minimum spatial wavelength Δt_0) is acceptable, then I prefer to put it explicitly into the calculation of rms slowness:

$$m = \{\frac{1}{t_0}\int_0^{t_0} [v(t_0') \ * \ \text{smooth}(t_0'/\Delta t_0)]^2 dt_0'\}^{-1} \ ,$$

where $\text{smooth}(x) = e^{-\pi x^2}$ for example.

I optimized the stacking velocity function in figure 12 with a steepest descent algorithm and explicit line searches. In the early iterations the semblance panel must be smoothed over slowness. Interval velocities were allowed to range between 2km/s and 7km/s. Δt_0 equaled 0.2s. The velocity function passes through most peaks of the semblance panel but avoids the inconsistent peak just before 2.5s.

Phase balancing of common-midpoint gathers

Having chosen a velocity function, we can now attempt to model the common-midpoint gather of figure 11 with convolutional wavelets and a single reflectivity function. I used four iterations of the previous algorithm to estimate the reflectivity function in figure 13a. Only the most important reflections are modeled in figure 13b by this reflectivity. The difference between the original and modeled data appear in figure 13c. Modeled changes in reflection strengths with offset do not entirely match those of the recorded data.

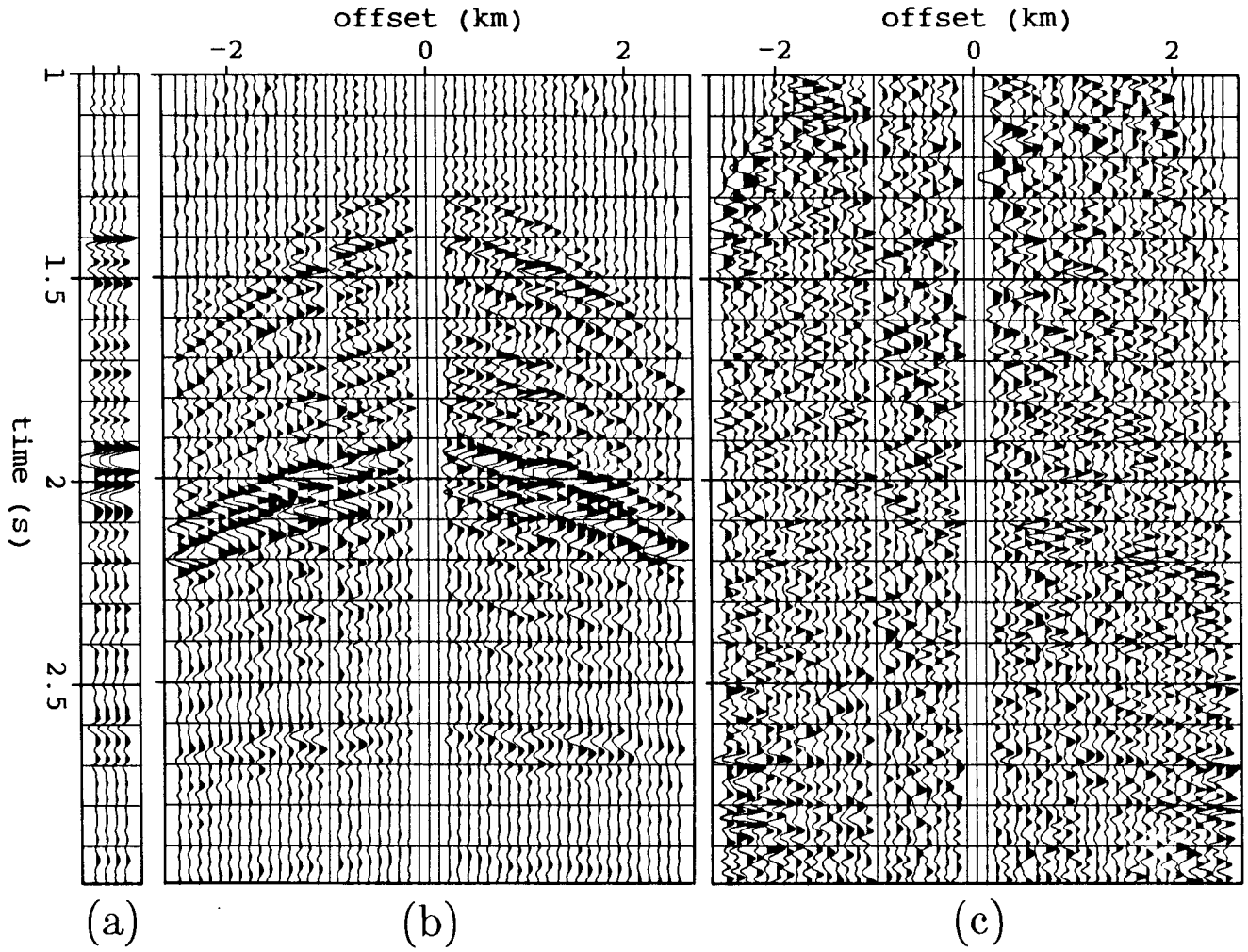

FIG. 13. (a) The estimated reflectivity function. (b) The corresponding modeled data. (c) The difference between the recorded and modeled data. Only the most important reflections are modeled, but static shifts are modeled well.

But the static shifts, our present goal, are modeled well. These static shifts show up clearly in the estimated wavelets in figure 14. When the original gather is deconvolved with these wavelets (figure 15), the resulting reflections are strikingly hyperbolic. A second velocity analysis (figure 16) is contoured at the same semblance values as figure 12. The reflections stack much more coherently than before.

How much of this increased hyperbolicity is reliable? The convolutional wavelets tried to accommodate the chosen velocity function, so the deconvolution naturally encourages hyperbolas that fit this function. On the other hand, the deconvolutions are one-dimensional, and the wavelets are short. There is no explicit mixing of information

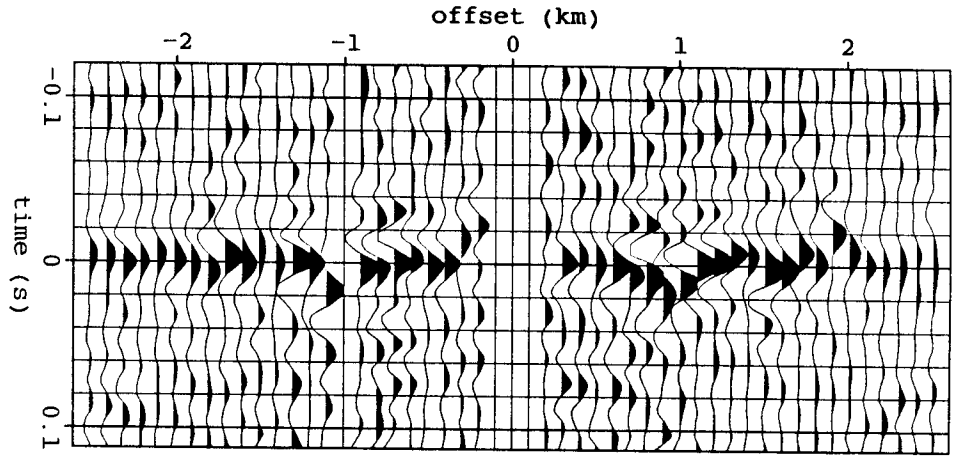

FIG. 14. Estimated convolutional wavelets for each trace. Static shifts are plainly visible.

across offset, so it is difficult to create reflections that did not exist. Only the hyperbolic curvature remains in doubt. Convolutions cannot alter the curvature of one reflection without altering the rest as well. The convolutions must explain as many reflections as possible, so random errors in the chosen velocity function should tend to cancel each other out.

In any event, I use the same velocity functions to stack (sum) the midpoint gathers over offset, so phase-balancing will make these stacks as coherent as possible. (A stacked section is a function of midpoint and zero-offset time.) Figure 17a shows the result of stacking 44 adjacent common-midpoint gathers with individually picked velocity functions. The velocity functions are smoothed over midpoint (by leaky integration) to avoid abrupt changes. All gathers are phase-balanced by deconvolution with individually estimated wavelets and stacked again (figure 17b). Although deconvolved traces are renormalized to the strength of the originals, the stacked traces increase in amplitudes by about 40%. Reflections are cleaner because shifted reflections no longer sum destructively. Each gather becomes internally consistent over offset after the phase-balancing deconvolution, but midpoint-consistent static shifts remain, thus the parallel appearance of the stacked reflections.

As an alternative stack, the estimated reflectivity functions for each gather are shown in figure 17c. The reflection at 2s has increased dramatically in amplitude with

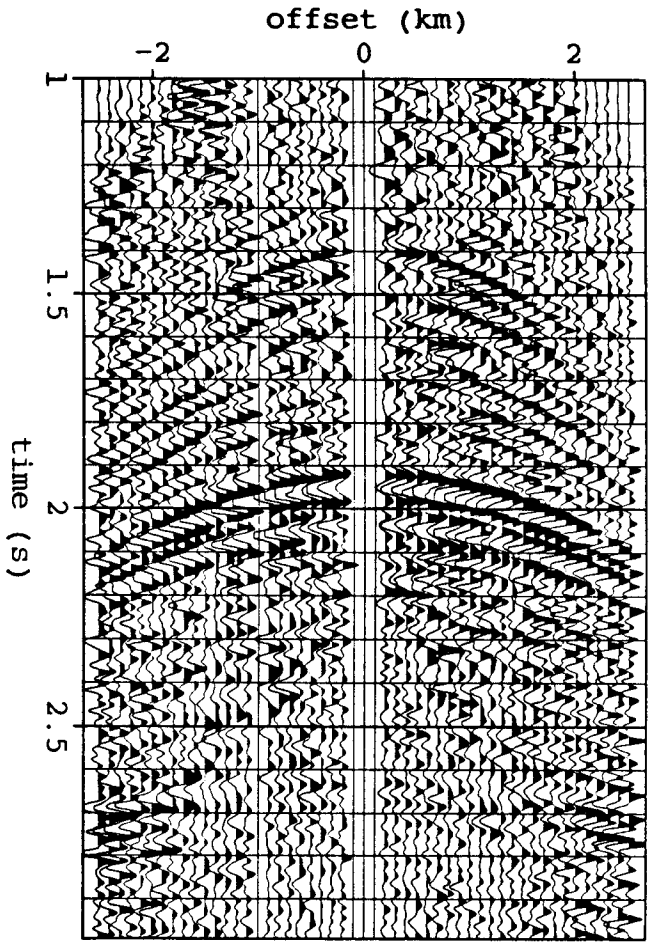

FIG. 15. Deconvolving the data in figure 11 with the estimated wavelets in figure 14 greatly enhances the hyperbolicity of the reflections.

respect to the other reflections. An extra double peak appears in this reflection as well. This double peak was visible in the midpoint gather in figure 11 (the third trace in the stack), but not in either stacked section (figures 17a and 17b). Stacking implicitly stretched and blurred the detail of this reflection. On the other hand, the reflection just before 2.5s corresponded to an unreasonably low (multiple?) velocity that was missed by the velocity function in figure 12. This event still contributes significantly to the stack in figure 17b because all hyperbolas are almost flat at low offsets. This reflection weakens in the estimated reflectivity in figure 17c because the corresponding modeled reflection must fit the data at all offsets. (Compare the synthetic examples in figures 5b and 6a).

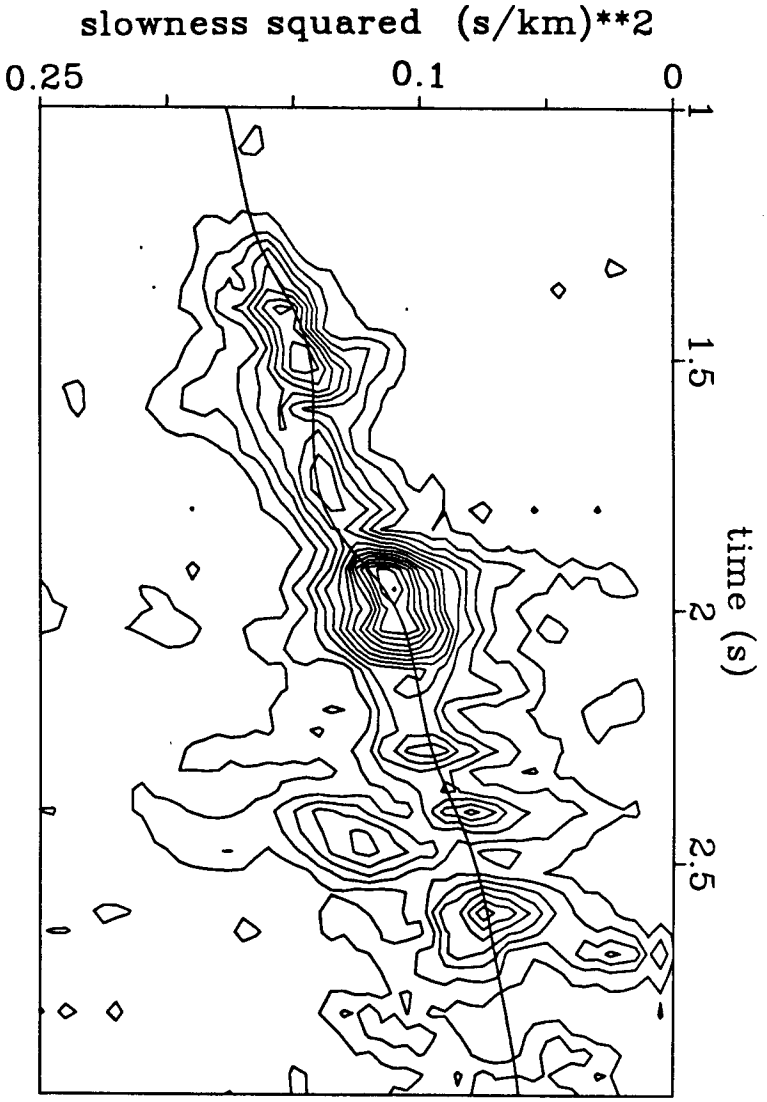

FIG. 16. A hyperbolic semblance stack of the phase-balanced data in figure 15 shows much higher resolution than before.

To see how midpoint-consistent the remaining static shifts are, each corresponding trace of the three stacked panels in figure 17 were shifted by equal amounts so as to maximize the flatness of the strongest reflectors (figure 18). Making one event flat indeed appears to make all reflections flatter. Estimating the residual midpoint-consistent static shifts requires additional physical constraints over midpoint.

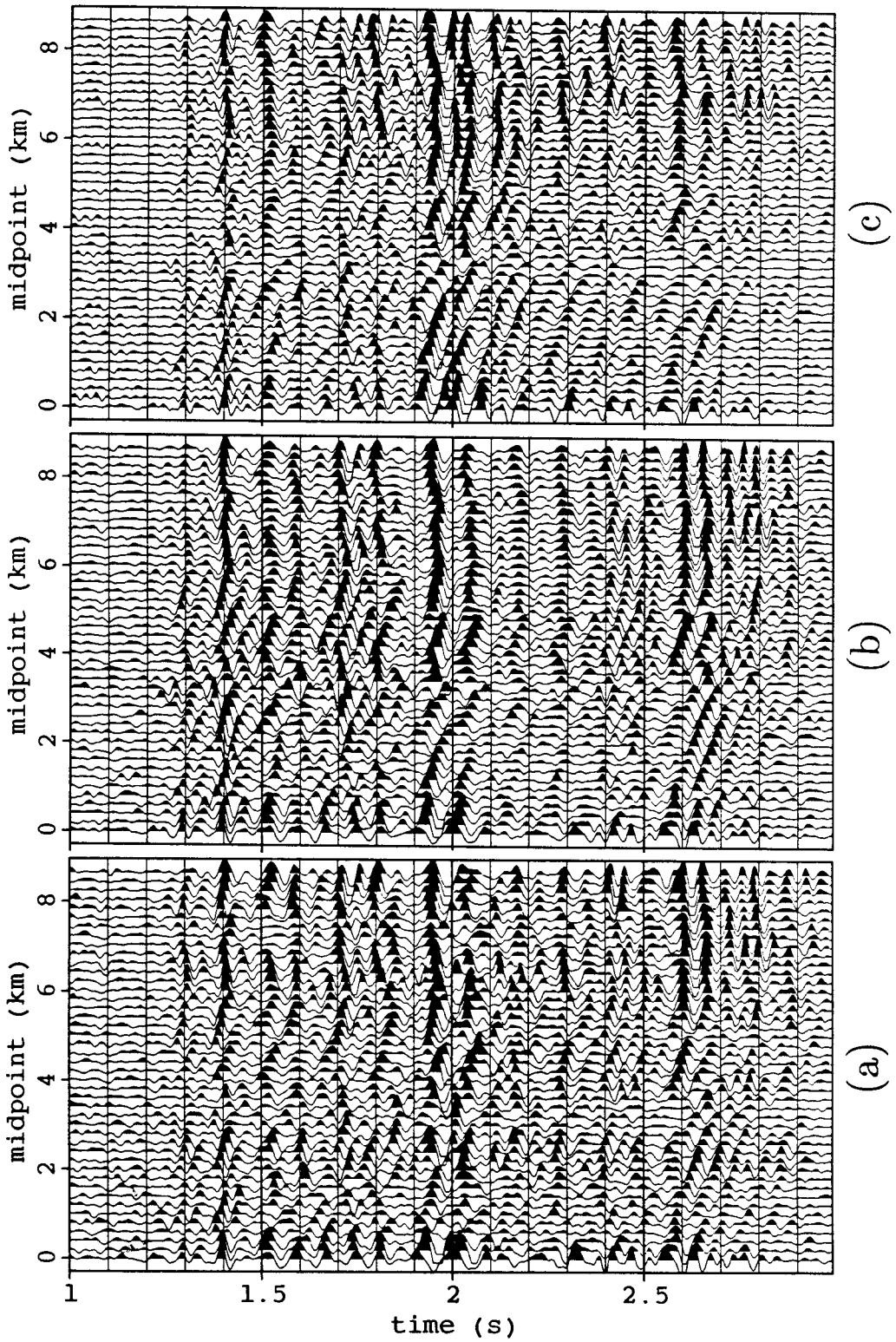

FIG. 17. (a) A stack of 44 adjacent midpoint gathers. (b) A stack of the same gathers after phase balancing. (c) The estimated reflectivity functions for the same gathers.

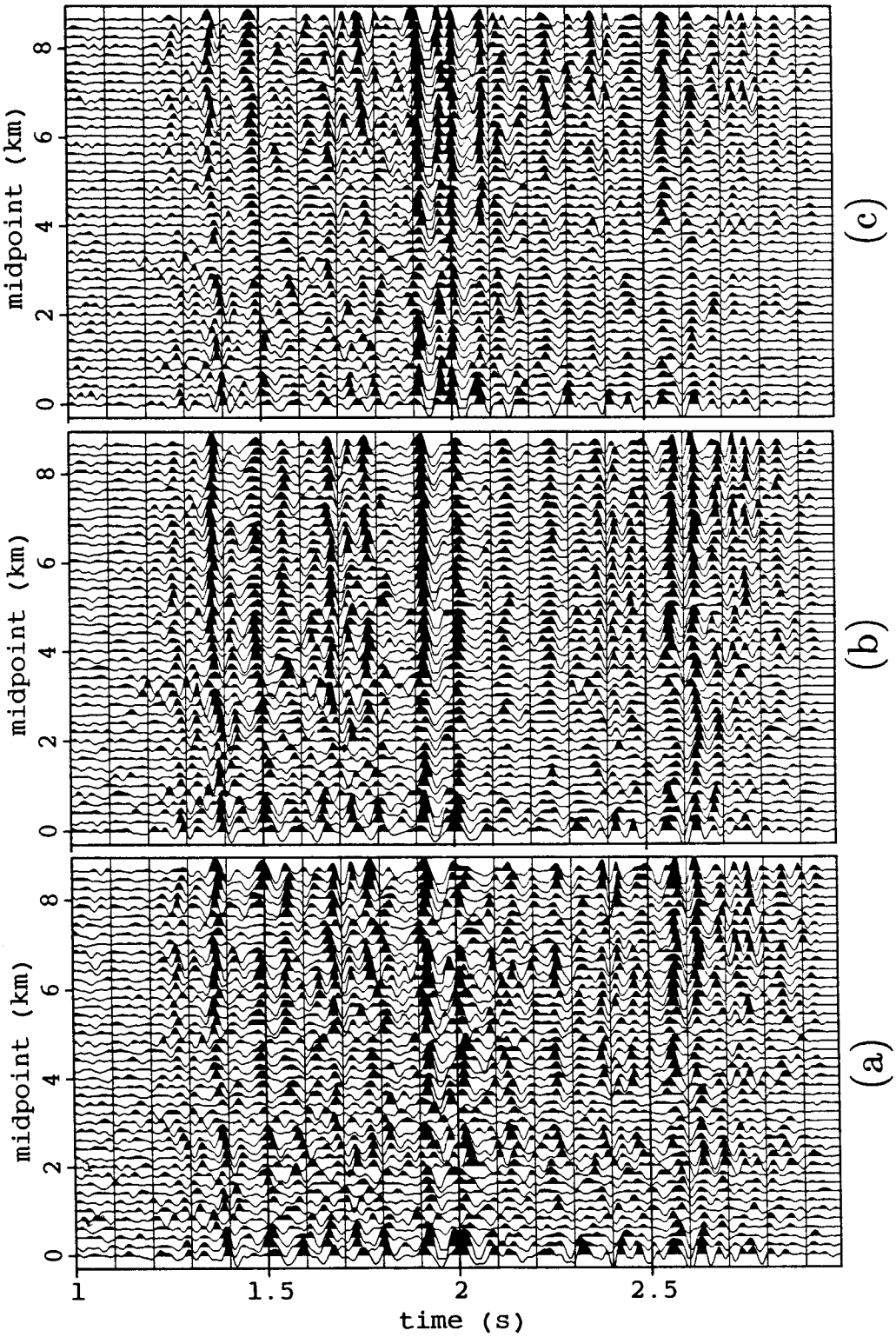

FIG. 18. The three panels of figure 17 after static shifts that flatten the strongest reflections. Residual static shifts appear to have been midpoint consistent.

CONSTRAINING REFLECTIONS OVER MIDPOINT

So far I have treated midpoint gathers as if they were independent. In fact they are linked by both their overlapping shot and geophone positions and their strongly correlated reflectivity functions. Surface-consistent filtering convolves each trace with wavelets at each shot and geophone position. If propagation velocities vary as smoothly laterally as we have assumed them to vary vertically, then reflections can be described as a sum of diffraction hyperbolas over midpoint.

Constrain wavelets or reflectivity?

Surface-consistency has been a popular constraint on prestack deconvolution and static corrections because it (1) reduces the dimensionality of unknowns and (2) encourages consistency and continuity over offset and midpoint. Reducing unknowns increases the data redundancy and helps the estimation of wavelets. Two one-dimensional arrays of wavelets replace one two-dimensional array. Spatial consistency makes the data more coherent for stacking and migration. The addition of strong physical constraints on reflections over offset has already made the first reason unnecessary. A similar constraint over midpoint could make the second reason unnecessary as well.

A simple experiment showed that surface consistency does not constrain the wavelets as much as one might hope. The wavelets estimated for the land data in the previous section were decomposed by least-squares into shot- and geophone-consistent wavelets. Deconvolution with this smaller set of wavelets had the same effect on the data as the original estimates: static shifts were corrected over offset but not over midpoint. When included in the decomposition, midpoint-consistent wavelets did little but scale amplitudes.

In a medium with gently varying velocities, zero-offset reflections can be described as a superposition of diffraction hyperbolas. Hyperbola curvatures are determined by velocities analogous to the rms values used for normal moveout. Rather than invert for reflectivity functions that vary arbitrarily with midpoint, one could invert for migrated sections, each point of which maps to a diffraction hyperbola over midpoint. The stacked sections in figure 17 would be difficult to create as a sum of hyperbolas. Migration, the inverse of diffraction, would interpolate across short gaps in reflectors and turn the edges of broken reflectors into large ellipses.

Surface-consistent estimation of the residual midpoint-consistent statics is limited to spatial wavelengths less than the range of offsets. The resolution obtained from constraints on reflectivity, on the other hand, depends on the width of diffraction hyperbolas, which become larger with depth.

A surface consistent model

Surface-consistent convolutions of traces are independent within a single midpoint gather (see equation [3]). Adjacent midpoint gathers duplicate most of the same shot and geophone positions, but each gather pairs the positions differently. (Midpoints usually divide into even and odds sets, each with an independent set of shots and geophone positions.)

Using more than one midpoint gather increases the available information, but wavelets must also be defined separately for shot and geophone locations. Reflectivity is a function of the midpoint y:

$$\text{hyp}_2(y,h,t) = \sum_j \int \delta[t - \sqrt{{t_0}^2 - h^2/{v_j}^2(y,t_0)}]\; r_j(y,t_0)\; dt_0 \text{ , and}$$

$$\hat{\text{data}}_2(s,g,t) = w_s(s,t) * w_g(g,t) * \text{hyp}_2[y=(s+g)/2,\; h=(g-s),\; t] \text{ .} \qquad (12)$$

The two-dimensional reflectivity functions $r_j(y,t_0)$ can be treated as unmigrated stacked sections, each corresponding to a different velocity function $v_j(y,t_0)$. An optimum stacked section can be interpolated through the alternative reflectivity functions. Notice that the model makes no assumptions about structure of the two-dimensional reflectivity functions.

A damped least-squares objective function similar to equation (6) defines an estimate of the unknowns, but the shot and geophone wavelets cannot easily be optimized simultaneously. As before, one could alternately estimate reflectivities and shot and geophone wavelets by holding the other two sets of parameters constant.

Deconvolving midpoint gathers independently avoids the programming difficulties of moving the larger data set in and out of computer memory. As a compromise, overlapping sets of two or more gathers could be deconvolved together.

Dip moveout corrections

Because reflections may be steeply dipping, the two-dimensional stacking velocity functions used in equation (12) cannot be used directly for the migration of the estimated reflectivity functions. Estimating reflectivity functions (or stacking data) with velocities corresponding to flat reflectors will filter out dipping events that show artificially higher stacking velocities (Hale, 1983b). A dip moveout (DMO) correction makes stacking velocities independent of the angle of reflection; corrected velocity functions become more continuous over time and midpoint.

Stacking velocity is related to the constant migration (propagation) velocity of a medium by the following "cosine correction" (Levin, 1971):

$$v_{\text{stack}} = v_{\text{mig}}/\cos\theta \tag{13}$$

θ is the angle of the dipping reflector from the horizontal. (Root-mean-square velocities describe low-order changes in traveltime with offset as though the medium were constant velocity.)

Simple geometry shows that the change in zero-offset traveltime with midpoint is also a function of the dip angle and medium velocity:

$$p = dt_0/dy = \sin\theta/v_{\text{mig}} \tag{14}$$

The combination of equations (13) and (14) with (1) produces the following moveout equation:

$$t^2 = t_0^2 + h^2/v_{\text{mig}}^2 - h^2p^2 \quad . \tag{15}$$

The reflections present at any particular dip can be separated by a linear dip filter of the reflectivity functions (e.g. Hale, 1983a). Dip filters are more easily defined in the frequency domain. For example:

$$r_j(y,t_0) \text{ Fourier transforms to } r'_j(k,f) \text{ , and}$$

$$\text{dipfil}_j(p,y,t_0) \text{ Fourier transforms to}$$

$$\text{dipfil}_j'(p,k,f) = \text{window}[(k/f - p)/\Delta p]\; r_j'(k,f) \; . \tag{16}$$

k and f are the Fourier duals of y and t_0 . window$(x) = e^{-\pi x^2}$, for example. The constant Δp gives the width of the dip filter. Each dip component can be modeled separately with the dip-corrected moveout equation and then added together to produce the desired impulsive hyperbolas:

$$\text{hyp}_3(y,h,t) =$$

$$\sum_p \sum_j \int \delta[t - \sqrt{t_0^2 + h^2/v_j(y,t_0)^2 - h^2p^2}\,]\; \text{dipfil}_j(p,y,t_0)\; dt_0. \tag{17}$$

Least-squares inversion of this modeling equation with respect to the reflectivity function is straightforward. The adjoint equation is just a hyperbolic stack, a dip filter, an adjustment of stacking velocities, and a sum of the different dip components. Now that migration velocities are used, one could use a migrated section to parametrize the two-dimensional reflectivity functions--thereby increasing the physical constraints on the data.

Other amplitude changes

The hyperbolic models (4) and (12) assume incorrectly that reflection amplitudes are constant with offset before surface filtering. Spreading of wavefronts will, however, decrease the amplitude with the distance propagated. If the data amplitudes are first scaled by the time traveled, this effect should be approximately balanced. Experiment has shown, however, that scaling by the second power of time comes closer to balancing amplitudes (the case with data used in this paper), perhaps because of the absorption of energy by an approximately constant Q material (Claerbout, 1985). Local rescaling of amplitudes (automatic gain control) distorts wavelets and so should be avoided.

The previous models also assume that reflection coefficients do not change with the angle of reflection. Convolutional wavelets cannot easily model angle-dependent changes for many reflections at once. Angle-dependent changes are much more visible over offset than over midpoint. Surface-consistent changes affect offset and midpoint equally. On the other hand, $r_i(t_0)$ could model such changes if it were made a smooth function of the radial parameter h/vt, roughly the tangent of the angle of reflection from the vertical.

A heterogeneous medium also affects amplitudes at intermediate depths between the surface and reflecting layers. Neither convolutional nor angle-consistent parameters are suited to the modeling of such changes. Kjartansson (1979) and Claerbout (1985) explain how these changes depend on offset and midpoint.

CONCLUSIONS

The combined modeling equations for hyperbolic reflections and convolutional filtering show what sort of data can be modeled by such parameters. The synthetic examples of inversion demonstrate what information about the parameters can be recovered from the data.

The parameters, though few, are flexible and immediately useful. The reflectivity functions can be treated as implicitly deconvolved stacked traces, often the final result of processing midpoint gathers. The convolutional wavelets model and allow removal of inconsistent changes in phase from trace to trace--changes that are usually parametrized as static shifts. The required velocity functions are the same as those required for stacking; however, the model can include additional velocity functions to model overlapping reflections with different curvatures.

When midpoint gathers are processed independently, no assumptions need be made about the changes in structure (reflectivity) from midpoint to midpoint. By contrast,

many static-correction algorithms must assume relatively flat dip. The convolutional wavelets have no explicit constraints except length. Optimization in the time domain avoids the issue of phase-unwrapping. The convolutional form avoids the local minima that arise when pure time shifts skip a cycle.

On the other hand, convolutional wavelets model only filtering of reflections near the surface, not at intermediate depths. For rms velocities to adequately parametrize reflection traveltimes, velocities must vary slowly with depth. The reflectivity functions, as defined, cannot explain any changes in reflections with offset or angle.

The optimization method allows wavelets to explain only what cannot be easily modeled by the reflectivity functions. The reflectivity can model relatively short consistent wavelets with a superposition of approximately parallel hyperbolas. The absolute phase of estimated wavelets is arbitrary--probably as close to zero phase as possible. After a phase-balancing deconvolution, statistical methods can attempt to estimate a single consistent wavelet for the entire gather.

The more exactly one constrains the velocity functions, the easier it is to distinguish the contributions of overlapping hyperbolas and inconsistent wavelets. On the other hand, a range of velocities allows one to model and suppress less desirable reflections, such as multiples. The structure of the modeling equations discourages simultaneous optimization of precise velocity functions.

The least-squares inversion uses only the simplest of possible statistical constraints. One could encourage simplicity and sparseness in the estimated stacked data, as do Thorson and Claerbout (1985) or Harlan (1986). Limiting the number of modeled hyperbolas would require wavelets to model more of the phase of short wavelets.

The number of physical parameters can be increased or decreased as suits the data or application. Gathers can be processed individually or in groups. Angular changes in amplitudes, time-adaptive wavelets, and migrated stacks can all be introduced with new parameters. This paper treats only two immediate applications of the combined hyperbolic and convolutional model. Most importantly, these examples show that the estimation of waveforms, structure, and velocities need not be pursued independently.

ACKNOWLEDGMENTS

Most of this work was completed at the Seismic Signal Processing Research Center in the automation department at Qinghua University in Beijing. The Geophysical Research Institute in Zhuoxian, China, supplied the marine data with multiples. Western Geophysical supplied the land data from the Williston basin. I thank the

Stanford Exploration Project and Fabio Rocca for allowing me to use their facilities for two months to complete this paper.

REFERENCES

Bracewell, R.N., 1978, The Fourier transform and its applications: McGraw Hill Book Company.

Claerbout, J.F., 1985, Imaging the earth's interior: Blackwell Scientific Publications.

Claerbout, J.F., 1986, Simultaneous pre-normal moveout and post-normal moveout deconvolution: Geophysics, 51, 1341-1354.

Hale, I.D., and Claerbout, J.F., 1983a, Butterworth dip filters: Geophysics, 48, 1033-1038.

Hale, I.D., 1983b, Dip-moveout by Fourier transform: Geophysics, 49, 741-757.

Harlan, W.S., 1986, Signal/noise separation and seismic inversion: Ph.D. thesis, Stanford University.

Hutchinson, D., and Link, B., 1984, Long period multiple suppression by model fitting: presented at the 54th Ann. Internatl. Mtg. and Expos., Soc. Explor. Geophys., Atlanta.

Kendall, M., and Stuart, A., 1979, The advanced theory of statistics, v.2, Inference and relationship, 4th ed.: Charles Griffin & Company Limited.

Kjartansson, E., 1979, Attenuation of seismic waves and applications in energy exploration: Ph.D. thesis, Stanford University.

Levin, F.K. 1971, Apparent velocity from dipping interface reflections: Geophysics, 36, 510-516.

Luenberger, D.G., 1984, Linear and nonlinear programming: Addison-Wesley Publishing Company, Inc.

Menke, W., 1984, Geophysical data analysis: discrete inverse theory: Academic Press, Inc.

Robinson, E.A., 1983, Seismic velocity analysis and the convolutional model: D. Reidel Publishing Company.

Ronen, J., and Claerbout, J.F., 1985, Surface-consistent residual statics by stack-power maximization: Geophysics, 50, 2759-2767.

Rothman, D.H., 1986, Automatic estimation of large residual statics corrections: Geophysics, 51, 332-346.

Thorson, J.R., and Claerbout, J.F., 1985, Velocity-stack and slant-stack stochastic inversion: Geophysics, 50, 2727-2741.

Toldi, J.L., 1985, Velocity analysis without picking: Ph.D. thesis, Stanford University.